Reprinted from

CMES

Computer Modeling in Engineering & Sciences

Founder and Editor-in-Chief:
Satya N. Atluri

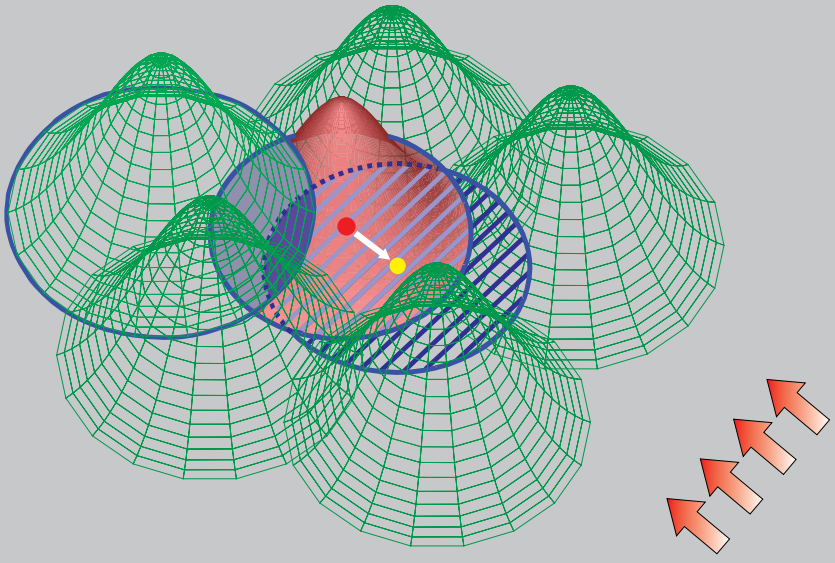

ISSN: 1526-1492 (print)
ISSN: 1526-1506 (on-line)

Tech Science Press

 CMES, vol.59, no.1, pp.31-63, 2010

Meshfree Point Collocation Schemes for 2D Steady State Incompressible Navier-Stokes Equations in Velocity-Vorticity Formulation for High Values of Reynolds Number

G.C. Bourantas[1], E.D. Skouras[2,3], V.C. Loukopoulos[4] and G.C. Nikiforidis[1]

Abstract: A meshfree point collocation method has been developed for the velocity-vorticity formulation of two-dimensional, steady state incompressible Navier-Stokes equations. Particular emphasis was placed on the application of the velocity-correction method, ensuring the continuity equation. The Moving Least Squares (MLS) approximation is employed for the construction of the shape functions, in conjunction with the general framework of the point collocation method. Computations are obtained for regular and irregular nodal distributions, stressing the positivity conditions that make the matrix of the system stable and convergent. The accuracy and the stability of the proposed scheme are demonstrated through two representative, well-known, and established benchmark problems. The numerical scheme was also applied to a case with irregular geometry for marginally high Reynolds numbers.

Keywords: Meshfree point collocation method, Velocity-vorticity formulation, 2D incompressible Navier-Stokes equations, Velocity correction method.

1 Introduction

Classical computational simulation techniques, such as the finite element methods (FEM) and the finite volume methods (FVM), are often used to model and investigate complex multi-physics phenomena arising in engineering systems. In these methods, the spatial domain is often discretized into meshes requiring a significant computational effort. In fact, for most models of geometrically intricate components, commonly encountered in engineering analysis, the mesh generation is sig-

[1] Department of Medical Physics, School of Medicine, University of Patras, GR 26500, Rion, Greece.
[2] Department of Chemical Engineering, University of Patras, GR 26500, Rion, Greece.
[3] Institute of Chemical Engineering and High Temperature Chemical Processes - Foundation for Research and Technology, P.O. Box 1414, GR-26504, Patras, Rion, Greece.
[4] Department of Physics, University of Patras, Patras, 26500, Rion, Greece.

nificantly time consuming and far from automated [Divo and Kassab (2006)]. It can be said with some level of assurance that, in most FVM or FEM analyses the mesh generation is the most taxing part of the modeling procedures, and quite often a mesh has to be adapted to the solution requiring an expensive re-meshing operation. Finite element methods, having been the most frequently used numerical methods in engineering during the past decades, have come to face certain inefficiencies in further development and optimization. More specifically, the lack of universally accepted and efficiently implemented 3D mesh generators poses severe difficulties in the unattended and robust calculation of the solution of many "stiff" 3D problems of technological value. It is generally accepted that due to their very nature, mesh-based methods are not well-suited for problems having large deformations and locally varying length scales [Liu (2002)], even with modern computational capacities.

Meshfree (or meshless) methods, are a class of numerical techniques that rely on interpolation/approximation on (non-ordered in general) spatial point distributions that offer the hope of reducing the effort devoted to model preparation significantly. Meshless techniques overcome the aforementioned difficulties associated with meshing by eliminating the mesh altogether. Interpolation/approximation is performed in terms of nodal points distributed at the analysis domain using functions having compact support. A weighted residual technique is used to generate the discrete set of equations corresponding to the governing partial differential equations. Several meshfree methods have been proposed since the prototype of the meshfree methods, the Smoothed Particle Hydrodynamics (SPH), was introduced [Gingold and Monaghan (1977)]. They are, namely, the Diffuse Approximation Method (DAM) [Nayroles, Touzot, and Villon (1991)], that is closely related to the moving least-squares method; the Diffuse Element Method (DEM) [Nayroles, Touzot, and Villon (1992)], developed by the moving least squares approximation and, the Element Free Galerkin method (EFG) [Belytschko, Lu and Gu (1994)]; the Reproducing Kernel Particle Method (RKPM) [Liu, Jun and Zhang (1995), Liu et al (1995)], which used to improve the SPH approximation; the Partition of Unity Finite Element Method (PUFEM) [Melenk and Babuska (1996)]; the *hp*-Clouds [Duarte and Oden (1996)]; the Moving Least-Square Reproducing Kernel Method (MLSRK) [Liu, Li and Belytschko (1996)]; the meshless Local Boundary Integral Equation Method (LBIE) [Zhu, Zhang and Atluri (1998)]; the Meshless Local Petrov–Galerkin method (MLPG) [Atluri, Kim and Cho (1999), Atluri and Shen (2002)]; the Finite Point method (FPM) [Onate, Idelsohn, Zienkiewicz and Taylor (1995)]; Meshless Point Collocation methods (MPC) [Aluru (2000)]; and more. It should be noted that most of these methods are not truly meshless, since they often need to use a background mesh for the numerical integration. However, the finite

point method, the point collocation method and the MLPG method are truly meshless methods. These methods, although still posing some issues in robustness and implementation, they inherently circumvent the connectivity and smoothly varying length scale requirements of mesh elements altogether and can be easily adapted to a plethora of physical domains.

Two methods of spatial discretization, namely the collocation method and the Galerkin method, have been dominant in existing meshless methods. Both methods are produced by the implementation of the weighted residuals method, which is one of the most widely applied procedures for solving numerically partial differential equations (PDEs). Until recently, Galerkin methods have been used extensively in the meshfree methods community. Successful implementation of Galerkin-formulated meshfree methods have reported in the fracture mechanics, compressible Euler [Liu, Jun, Sihling, Chen and Hao (1997), Ahn, Chang, Choe and Kim (2006)] and Navier-Stokes equations [Gunther, Liw and Diachin (2000)], incompressible flow problems [Choe, Kim, Kim and Kim (2001)], and more. Despite the fact that Galerkin-based meshfree methods have many advantageous features, the difficulties of imposing essential boundary conditions, along with the necessity for background cells for the Galerkin formulation, raise several difficulties during the implementation of the method. On the other hand, the collocation method solves the strong form of the partial differential equations. The solution obtained is commonly referred to as the "strong" solution. Recent advances [Zhang, Liu, Song and Lu (2001), Aluru (2000), Mai-Duy and Tran-Cong (2001), Mai-Duy and Tran-Cong (2001)] on meshless point collocation (MPC) methods have shown encouraging results which signify the reliability of the method. The most important advantage of this method is that it requires no mesh or grid prescriptions at all. Hence, MPC is a truly meshless method, compared to Galerkin-based meshfree methods.

Many theoretical and numerical studies have been published for the fundamental problem in fluid mechanics, that is, the solution of incompressible Navier-Stokes equations. For this system of coupled partial differential equations there are three types of formulation, the formulation of the primitive variables ($\boldsymbol{u}$, p), the velocity-vorticity formulation ($\boldsymbol{u}$, ω) and the streamfunction-formulation (ψ, ω). The first two formulations can be used yet for problems in three dimensions, while the last can be used only for two-dimensional problems. In regard to the primitive variables formulation, there is a significant limitation, termed the inf-sup (or LBB) condition, which prevents the efficient approximation of the velocity and the pressure field [Brezzi (1974), Babuska (1973)]. This means that numerical instability, along with the presence of some spurious pressure values, is effectively inevitable [Babuska (1971)]. To overcome this shortcoming, two sets of elements for the Galerkin-based methods (or FDM) have to be implemented, in order to satisfy the

inf-sup condition. The construction of such elements is an important issue, and special elements have been devised for the continuous pressure approximation, such as the mini elements [Arnold and Liu (1995)], and the Taylor-Hood [Taylor and Hood (1973)] elements. On the other hand, the dual grid sets due to the inf-sup condition can be circumvented through the velocity-vorticity formulation of the Navier-Stokes equations. Velocity-vorticity formulation does not suffer from the inf-sup condition, but it experiences other type of difficulties arising from the implementation of the vorticity boundary conditions [Weinan and Liu (1996)]. Since the vorticity is generated from the wall due to viscosity, there have been numerous efforts to compute accurately the vorticity on the wall. In particular, the implementation of the vorticity boundary conditions in the framework of collocation-based meshfree scheme has been seen in a limited number of recent works [Kim, Kim, Jun and Lee (2007)].

A brief survey on some of the most significant studies which use different types of meshless numerical methods on the solution of the Navier-Stokes equations will be given next. In doing so, the emphasis will be focused on three points: on the meshless numerical method used (strong or weak form), on the interpolation/approximation function (shape function) used, and on the largest Reynolds number achieved. To the authors' best knowledge, in all these studies the maximum Reynolds number achieved for the 2D steady incompressible flow in a lid-driven cavity is no more than 15000. In these works, several benchmark problems have been used in order to demonstrate the accuracy of a proposed scheme. Two of the most popular problems considered are the well-established lid-driven square cavity flow and the backward-facing step flow. More precisely, the work on MLPG [Lin and Atluri (2001)] solved the incompressible Navier-Stokes equations for the lid-driven benchmark problem, up to $Re = 400$. The local weak form was modified in a very careful way so as to overcome the so-called LBB conditions. In addition, the up-winding scheme was used to stabilize the convection operator in the streamline direction. Furthermore, the truly Meshless Local Petrov-Galerkin (MLPG) method was extended for computation of steady incompressible flows, governed by the Navier–Stokes equations (NSE), in vorticity-stream function formulation [Mohammadi (2008)]. The proposed method is a truly meshless method based on only a number of randomly located nodes. The formulation was based on two equations including stream-function Poisson equation and vorticity advection-dispersion-reaction equation (ADRE). The meshless method was based on a local weighted residual method with the Heaviside step function and quartic spline as the test functions respectively over a local subdomain. Radial basis functions (RBF) interpolation was employed in shape function and its derivatives construction for evaluating the local weak form integrals. Moreover, a stabilization procedure,

based on a modification of SUPG, used in order to handle convection dominant flows in connection with the lid-driven cavity problem. For the lid-driven cavity benchmark problem Reynolds number used was up to $Re = 10000$. In [Arefmanesh, Najafi and Abdi (2008)] the meshless local Petrov-Galerkin (MLPG) method, along with unity as the weighting function, has been applied to the solution of the Navier-Stokes and energy equations. The Navier-Stokes equations in terms of the stream function and vorticity formulation together with the energy equation are solved for different test cases. The study considers the implementation of the method on a non-isothermal lid-driven cavity flow, the lid-driven cavity flow with an inlet and outlet, and also on the non-isothermal flow over an obstacle. Non-uniform point distribution was employed for all the test cases for the numerical simulations. Additionally, in [Baez and Nicolas (2009)] authors solved numerically the unsteady Navier-Stokes equations in primitive variables that govern viscous incompressible fluid flow. A simple projection method was used, which involves an operator splitting technique of three steps in the time discretization process. The proposed numerical scheme does not involve any iteration, is independent of the spatial dimension and, its costly part relies on the solution of elliptic problems for which very efficient solvers exist regardless of the spatial discretization. The scheme was tested with the well known two-dimensional lid-driven cavity problem at moderate and high Reynolds numbers Re in the range $400 \leq Re \leq 15000$. Authors in [Grimaldi, Pascazio, and Napolitano (2006)] used a numerical method for solving two- and three-dimensional unsteady incompressible flows. The vorticity-velocity formulation of the Navier–Stokes equations was considered, employing the vorticity transport equation and a second-order Poisson equation for the velocity. Furthermore, second-order-accurate centred finite differences on a staggered grid were used for the space discretization while the vorticity equation was discretized in time using a fully implicit three-level scheme. At each physical time level, a dual-time stepping technique was used to solve the coupled system of non linear algebraic equations by various efficient relaxation schemes. Steady flows were computed by dropping the physical time derivative and converging the pseudo-time-dependent problem. The application of the mesh-free Local Radial Basis Function Collocation Method (LRBFCM) in solution of coupled heat transfer and fluid flow problems in Darcy porous media was examined in [Kosec and Sarler (2008)]. The involved temperature, velocity and pressure fields were represented on overlapping sub-domains through collocation by using multiquadrics Radial Basis Functions (RBF). The involved first and second derivatives of the fields were calculated from the respective derivatives of the RBF's. The energy and momentum equations were solved through explicit time stepping. The pressure-velocity coupling was calculated iteratively, with pressure correction, predicted from the local continuity equation violation. Then, in [Mai-Duy and Tran-Cong (2001)] radial basis function networks

were used for solving steady incompressible viscous flow problems. The method used a 'universal approximator' based on neural network methodology to represent the solutions. For the square cavity flow the Reynolds number used reached the value $Re = 400$ for a grid density of 33×33. The authors in [Mai-Duy, Mai-Cao and Tran-Cong (2007)] utilized an indirect/integrated radial-basis-function network (IRBFN) method in order to solve transient partial differential equations (PDEs) governing fluid flow problems. Spatial derivatives were discretized using one- and two-dimensional IRBFN interpolation schemes, whereas temporal derivatives were approximated using a method of lines and a finite difference technique. Another approach was used in [Mariani, Alonso and Peters (2008)], where an application of Newton's method for linearization of advective terms given by the discretization on unstructured Voronoi meshes for the incompressible Navier-Stokes equations was proposed and evaluated. One of the major advantages of the unstructured approach is its application to very complex geometrical domains and the mesh is adaptable to features of the flow. Furthermore, 2D incompressible viscous flows from the unsteady Navier-Stokes equations in streamfunction–vorticity variables were presented [Nicolás and Bermúdez (2004)]. The results were obtained using a simple numerical procedure based on a fixed point iterative process to solve the nonlinear elliptic system that results once a second order time discretization was performed. Flows on the unregularized unit driven cavity were reported up to Reynolds numbers $Re = 20000$. The same authors [Nicolás and Bermúdez (2007)], solved the unsteady Navier-Stokes equations in its velocity-vorticity formulation. The results were obtained using a simple numerical procedure based on a fixed point iterative process to solve the nonlinear elliptic system that results once a second order time discretization is performed. Flows on the un-regularized unit driven cavity problem are reported up to Reynolds numbers $Re = 10000$.

In [Chinchapatnam, Djidjeli and Nair (2007)] the authors used the global Radial Basis Function along with the point collocation method, and they solved the laminar, incompressible Navier-Stokes in streamfunction–vorticity formulation for the lid-driven cavity benchmark problem up to Reynolds number $Re = 3200$, using a relatively coarse grid of 61×61 regular distributed nodes. The backward-facing step problem was solved also for $Re = 200$. The streamfunction-vorticity formulation was also used in [Kim, Kim, Jun and Lee (2007)], where the Reynolds number was set up to $Re = 1000$ in the case of lid-driven cavity flow. Therein, particular emphasis was placed on the novel formulation of effective vorticity conditions on the no-slip boundaries. Additionally, flow problems with complex geometry were also considered. Furthermore, a local radial basic function (RBF) based grid-free scheme was developed to solve the unsteady, incompressible Navier–Stokes equations in primitive variables [Sanyasiraju and Chandhini (2008)]. The velocity-

pressure decoupling was obtained by making use of a fractional step algorithm. The Reynolds number reached the value of $Re = 3200$ for the lid-driven cavity problems, although the number of nodes used reached the value of 113953. The Reynolds number for the step problem was set to $Re = 800$. In [Sellountos and Sequeira (2008)] the Local Boundary Integral Method (LBIE) was applied to solve both the aforementioned benchmark problems for $Re = 1000$ and $Re = 400$, respectively. Adiitionally, authors in [Sellountos and Sequeira (2008)] used a hybrid velocity-vorticity scheme for the solution of the 2D Navier- Stokes equations. The multi-region Local Boundary Integral Equation (LBIE) combined with Radial Basis Functions (RBF) interpolation was used for the solution of the kinematics and the multi-region BEM for the solution of the transport kinetics. For the lid-driven case results were presented for Reynolds number up to 3200, while for the backward-facing step Reynolds number was set to 200. Local radial basis function-based differential quadrature (RBF-DQ) method was proposed [Shu, Ding and Yeo (2005)]. The method was a natural mesh-free approach. The proposed scheme can be regarded as a combination of the conventional differential quadrature (DQ) method with the radial basis functions (RBFs) by means of taking the RBFs as the trial functions in the DQ scheme. Therein, three two-dimensional cases were tested, which were the driven-cavity flow, flow past one isolated cylinder at moderate Re number, and flow around two staggered circular cylinders. Regarding the lid-driven cavity the Reynolds number used was $Re = 5000$. Conjugate heat transfer problems modeled by convecting fully viscous incompressible fluid interacting with conducting solids were considered in [Divo and Kassab (2006)]. The meshless formulation for fluid flow modeling was based on a radial basis function interpolation using inverse Multiquadrics and a time-progression decoupling of the equations using a Helmholtz potential. Reynolds number $Re = 400$ was used for the lid-driven square cavity problem.

In the present paper we effectively incorporate the meshfree point collocation method into the velocity-vorticity description of 2D Stokes flows. The Moving Least Squares method for the approximation of the field variable is applied. An exponential weight function is used for the construction of the approximated function, which is applied on a constant number of support domain nodes, instead of a constant node density support domain. A key point for a wider use of the meshless point collocation method is the accuracy and the convergence of the obtained solution. Recently, the maximum principle for the discrete harmonic operator in the meshfree point collocation method has been proven [Kim and Liu (2006)], and the convergence proof for the numerical solution of the Poisson problem has been attained, accordingly. The collocation-based meshfree approach does not require any grid mesh, except of a set of regular or irregular distributed nodes in the spatial domain, ensuring the

positivity conditions. Thus, when it comes to a complex geometry, this method may have advantages over FDM, FEM and, even, other meshfree methods which need background cells for numerical integration. A regular nodal distribution embedded to complex geometries can be employed. Random point distributions (cloud points) can, and have, also been used; however, their robust convergence is not yet guaranteed under all configurations [Kim, Kim, Jun and Lee (2007)], but only when the positivity conditions were ensured [Aluru, N. (2000)]. In the present work, solutions for high values of the Reynolds number (up to 10000) have been attained, by the proper incorporation of a velocity correction technique into MPC method.

The paper is presented as follows. In Section 2, the moving Least Squares (MLS) approximation is briefly introduced. The velocity-vorticity formulation based on the meshfree point collocation method is next developed in Section 3, where the implementations of a velocity correction technique and the vorticity boundary conditions are emphasized. In Section 4, several numerical examples are presented for steady-state flow, which will demonstrate the performance of the method. Finally, discussions and conclusions complete the paper.

2 Moving Least Squares Approximation

2.1 Methodology

It is assumed that there are N discrete points located at $\mathbf{x} = \mathbf{x}_1, \mathbf{x}_2, ..., \mathbf{x}_N$ in the spatial domain Ω, where $\mathbf{x}_i = (x_i, y_i)$, $i = 1, 2, ..., N$. In the moving least-squares technique, the approximation $u^h(\mathbf{x})$ is expressed as the inner product of a vector of the polynomial basis $\mathbf{p}(\mathbf{x})$ and a vector of the coefficients $\mathbf{a}(\mathbf{x})$,

$$u^h(\mathbf{x}) = \mathbf{p}^T(\mathbf{x})\mathbf{a}(\mathbf{x}), \tag{1}$$

where $\mathbf{p}(\mathbf{x}) \in \mathrm{R}^m$, $\mathbf{a}(\mathbf{x}) \in \mathrm{R}^m$ and m is the number of monomials in the polynomial bases. The local character of the moving least-squares (MLS) approximation can be viewed as a generalization of the traditional least-squares approximation in which the vector $\mathbf{a}$ is not a function of $\mathbf{x}$. The polynomial basis can be written as $\mathbf{p}^T(\mathbf{x}) = \mathbf{p}^T(\mathbf{x} - \mathbf{x}_i) = \left[1, (x - x_i), (y - y_i), (x - x_i)^2, (x - x_i)(y - y_i), (y - y_i)^2, ..., (x - x_i)^m\right]$ in 2D problems. Herein, we used a second order $(m = 2)$ polynomial basis, obtaining $\mathbf{p}^T(\mathbf{x}) = \left[1, (x - x_i), (y - y_i), (x - x_i)^2, (x - x_i)(y - y_i), (y - y_i)^2\right]$.

Equation (1) is referred to as the global least-squares approximation. In addition, there exists a unique local approximation associated with each point in the domain.

In order to determine the form of $\mathbf{a}(\mathbf{x})$, a weighted discrete error norm,

$$J(\mathbf{x}) = \sum_{I=1}^{n} w_I(\mathbf{x}) \left[\sum_{j=1}^{m} p_j^T(\mathbf{x}_I)\, a(\mathbf{x}) - u_I \right]^2 \tag{2}$$

is constructed and minimized. Here, $w_I(\mathbf{x})$ denotes the weight function, $w_I(\mathbf{x}) \equiv w(\mathbf{x}-\mathbf{x}_I)$, associated with node I, and the quantity in brackets is the difference between the local approximation at node I and the data at node I, u_I, n is the number of nodes in the support of $w_I(\mathbf{x})$. The minimization of Eq. (2) with respect to $a(\mathbf{x})$ determines $\mathbf{a}(\mathbf{x})$. The local approximation associated with point $\mathbf{x}$ is used only in the minimization process and is equivalent to the global approximation at the single point $\mathbf{x}$. Compact support of the weight functions gives the moving least-squares method its local character.

2.2 Shape functions and their derivatives

The minimization of Eq. (2),

$$\frac{\partial J(\mathbf{x})}{\partial \mathbf{a}(\mathbf{x})} = 0, \tag{3}$$

results in the linear system

$$\mathbf{A}(\mathbf{x})\mathbf{a}(\mathbf{x}) = \mathbf{B}(\mathbf{x})\mathbf{U}_s, \tag{4}$$

where $\mathbf{U}_s$ is a vector containing the nodal data, $\mathbf{U}_s^T = [u_1, u_2, ..., u_n]$, and

$$\mathbf{A}(\mathbf{x}) = \sum_{I=1}^{n} w_I(\mathbf{x}) p(\mathbf{x}_I)\, p^T(\mathbf{x}_I), \tag{5}$$

$$\mathbf{B}(\mathbf{x}) = \left[w_1(\mathbf{x})\mathbf{p}(\mathbf{x}_1) \quad w_2(\mathbf{x})\mathbf{p}(\mathbf{x}_2) \quad ... \quad w_n(\mathbf{x})\mathbf{p}(\mathbf{x}_n) \right], \tag{6}$$

where $\mathbf{A} \in \mathrm{R}^{m\times m}$ and $\mathbf{B} \in \mathrm{R}^{m\times n}$. The matrix $\mathbf{A}$ must be inverted at every sampling point. Substitution of the solution of Eq.(4) into the global approximation Eq.(1) completes the least-squares approximation

$$u^h(\mathbf{x}) = \underbrace{\mathbf{p}^T(\mathbf{x})\mathbf{A}^{-1}(\mathbf{x})\mathbf{B}(\mathbf{x})}_{\varphi(\mathbf{x})}\mathbf{U}_s. \tag{7}$$

Here, the spatial dependence has been lumped into one row matrix, $\boldsymbol{\varphi}(\mathbf{x})$, and, therefore, the approximation takes the form of a product of a matrix of shape functions with a vector of nodal data. Derivatives of the shape functions may be calculated by applying the product rule to

$$\boldsymbol{\varphi} = \mathbf{p}^T\mathbf{A}^{-1}\mathbf{B}. \tag{8}$$

In order to obtain the spatial derivatives of the approximation function $u^h(\mathbf{x})$, it is necessary to obtain the derivatives of the MLS shape functions $\varphi_i(\mathbf{x})$,

$$\frac{\partial}{\partial x_j}u^h(\mathbf{x}) = \frac{\partial}{\partial x_j}\sum_{i=1}^{n}\varphi_i(\mathbf{x})u_i = \sum_{i=1}^{n}\left\{\frac{\partial}{\partial x_j}\varphi_i(\mathbf{x})\right\}u_i, \quad x_j = x,y,z. \tag{9}$$

The derivative of the shape function is given as

$$\frac{\partial\phi_i(\mathbf{x})}{\partial x_j} = \frac{\partial\left(\mathbf{p}^T\mathbf{A}^{-1}\mathbf{B}_i\right)}{\partial x_j} = \frac{\partial\mathbf{p}^T}{\partial x_j}\mathbf{A}^{-1}\mathbf{B}_i + \mathbf{p}^T\frac{\partial\left(\mathbf{A}^{-1}\right)}{\partial x_j}\mathbf{B}_i + \mathbf{p}^T\mathbf{A}^{-1}\frac{\partial\mathbf{B}_i}{\partial x_j}, \quad x_j = x,y,z, \tag{10}$$

where $\frac{\partial\left(\mathbf{A}^{-1}\right)}{\partial x_j} = -\mathbf{A}^{-1}(\mathbf{x})\frac{\partial\mathbf{A}(\mathbf{x})}{\partial x_j}\mathbf{A}^{-1}(\mathbf{x})$. Regarding the second order derivative of the unknown function one gets

$$\begin{aligned}
&\frac{\partial^2\varphi(\mathbf{x})}{\partial x_j^2} = \frac{\partial}{\partial x_j}\left(\frac{\partial\varphi(\mathbf{x})}{\partial x_j}\right) = \frac{\partial}{\partial x_j}\left(\frac{\partial\mathbf{p}^T}{\partial x_j}\mathbf{A}^{-1}\mathbf{B}_i + \mathbf{p}^T\frac{\partial\left(\mathbf{A}^{-1}\right)}{\partial x_j}\mathbf{B}_i + p^T\mathbf{A}^{-1}\frac{\partial\mathbf{B}_i}{\partial x_j}\right) = \\
&= \frac{\partial^2\mathbf{p}^T}{\partial x_j^2}\mathbf{A}^{-1}\mathbf{B}_i + \frac{\partial\mathbf{p}^T}{\partial x_j}\frac{\partial\left(\mathbf{A}^{-1}\right)}{\partial x_j}\mathbf{B}_i + \frac{\partial\mathbf{p}^T}{\partial x_j}\mathbf{A}^{-1}\frac{\partial\mathbf{B}_i}{\partial x_j} + \\
&+ \frac{\partial\mathbf{p}^T}{\partial x_j}\frac{\partial\left(\mathbf{A}^{-1}\right)}{\partial x_j}\mathbf{B}_i + \mathbf{p}^T\frac{\partial^2\left(\mathbf{A}^{-1}\right)}{\partial x_j^2}\mathbf{B}_i + \mathbf{p}^T\frac{\partial\left(\mathbf{A}^{-1}\right)}{\partial x_j}\frac{\partial\mathbf{B}_i}{\partial x_j} + \\
&+ \frac{\partial\mathbf{p}^T}{\partial x_j}\mathbf{A}^{-1}\frac{\partial\mathbf{B}_i}{\partial x_j} + p^T\frac{\partial\left(\mathbf{A}^{-1}\right)}{\partial x_j}\frac{\partial\mathbf{B}_i}{\partial x_j} + p^T\mathbf{A}^{-1}\frac{\partial^2\mathbf{B}_i}{\partial x_j^2},
\end{aligned} \tag{11}$$

where $x_j = x,y,z$ and $\frac{\partial^2\left(\mathbf{A}^{-1}\right)}{\partial x_j^2} = -\frac{\partial\left(\mathbf{A}^{-1}\right)}{\partial x_j}\mathbf{A}\mathbf{A}^{-1} - \mathbf{A}^{-1}\frac{\partial\mathbf{A}}{\partial x_j}\mathbf{A}^{-1} - \mathbf{A}^{-1}\mathbf{A}\frac{\partial\left(\mathbf{A}^{-1}\right)}{\partial x_j}$.

2.3 Weight Function

The weight function is non-zero over a small neighborhood of $\mathbf{x}_i$, called the support domain of node i. The choice of the weight function $W(\mathbf{x}-\mathbf{x}_i)$ affects the resulting approximation $u^h(\mathbf{x}_i)$ significantly. In the present paper a Gaussian weight function is used [Liu (2002), Bourantas, Skouras and Nikiforidis (2009)], yet the support domain does not have a standard point density value. Instead, a constant number of nodes are used for the approximation of the field function.

$$W(\mathbf{x}-\mathbf{x}_i) \equiv W(d) = \left\{\begin{matrix} e^{-\left(\frac{d_I}{a}\right)^2} \\ 0 \end{matrix}\right\}, \tag{12}$$

where $I = 1,2,3,...,q$ are the nodes that produce the support domain of node $\mathbf{x}_i$, and $d = \frac{|\mathbf{x}-\mathbf{x}_i|}{a_0^2}$ with a_0 a prescribed constant (often $a_0 = 0.2$).

3 Governing equations and solution procedure

3.1 Governing equations

Incompressible, steady state, fluid flow is governed by the Navier–Stokes equations, a well-known coupled set of nonlinear partial differential equations expressing the conservation of mass and linear momentum for a Newtonian fluid. In conservative form [Ligget (1994)], these equations are:

$$\mathbf{u}\cdot\nabla\mathbf{u} = -\nabla p + \frac{1}{Re}\nabla^2\mathbf{u} + \mathbf{f}, \tag{13a}$$

$$\nabla\cdot\mathbf{u} = 0, \tag{13b}$$

where $\mathbf{u}$ is the flow velocity vector, p is the field pressure, $\mathbf{f}$ is a specific body force and Re is the Reynolds number. All field variables are functions of space $\mathbf{x}$, in a fixed domain Ω surrounded by a closed boundary $\partial\Omega$. Equations (13a) and (13b) represent the Navier-Stokes equations in the velocity-pressure formulation. The vorticity vector $\boldsymbol{\omega}$ can be expressed as

$$\boldsymbol{\omega} = \nabla\times\mathbf{u}. \tag{14}$$

By taking the curl of both sides of Equation (13a) and using Equations (13b) and (14), we can obtain the vorticity transport equation:

$$\mathbf{u}\cdot\nabla\boldsymbol{\omega} = \boldsymbol{\omega}\cdot\nabla\mathbf{u} + \frac{1}{Re}\nabla^2\boldsymbol{\omega}. \tag{15}$$

Taking the curl of Equation (14) and using Equation (13b) we get

$$\nabla^2\mathbf{u} = -\nabla\times\boldsymbol{\omega}, \tag{16}$$

which is the vector form of the Poisson's equation for $\mathbf{u}$. Equations (15) and (16), with $\mathbf{u}$ and $\boldsymbol{\omega}$ as velocity and vorticity vectors, are known as the velocity-vorticity formulation of the Navier-Stokes equations and can replace Equations (13a) and (13b) in which $\mathbf{u}$ and p are primitive variables.

For the two-dimensional, steady state problems, if (u,v) are the velocity components and ω is the associated vorticity, then the vorticity transport equation, Equation (15), can be written as

$$\mathbf{u}\cdot\nabla\omega = \frac{1}{Re}\nabla^2\omega \tag{17}$$

and Equation (16) as

$$\nabla^2 u = -\frac{\partial \omega}{\partial y}, \tag{18}$$

$$\nabla^2 v = \frac{\partial \omega}{\partial x}. \tag{19}$$

The solution of the vorticity-transport equation (17), in combination with the velocity Poisson equations (18) and (19) with the prescribed boundary conditions, gives the velocity and the vorticity distribution all over the domain. For the velocity-vorticity formulation, even though the continuity equation has been assumed to be satisfied for the derivation of velocity Poisson equations, it may not be necessarily guaranteed. Thus, in order the continuity equation to be satisfied, the velocity correction method is applied.

3.2 Solution Procedure

Herein, an iterative scheme is utilized for the solution of the velocity-vorticity formulation of the Navier-Stokes equations. In the majority of the incompressible flow problems modeled with Navier-Stokes equations the most natural boundary conditions arises when the velocity is prescribed all over the boundaries of the problem. The vorticity boundary conditions are determined iteratively from computations. The iterative solution algorithm used for the discretized fluid flow set of Eqs. (17) - (19), must ensure coupled satisfaction of all the equations at convergence. We follow the approach of the so-called MAC algorithm proposed in [Harlow and Welch (1965) and used also in [Divo and Kassab (2006)]) in its primitive variables $(u-v-p)$ formulation. The process initiates from an initial velocity condition $u^{(0)}$ that satisfies the continuity equation (13b) within the entire problem domain $\Omega(x,y)$, that is, $\nabla \cdot \mathbf{u}^{(0)} = 0$. Following, the velocity-Poisson equation is solved using the point collocation method by taking known vorticity components. A new velocity field $u^{(*)}$ may be estimated from the velocity-Poisson equations. However, the solutions to the velocity-Poisson equations and corresponding boundary conditions of the vorticity fluxes, namely $\frac{\partial \omega}{\partial y}$ and $\frac{\partial \omega}{\partial x}$, do not necessarily satisfy the continuity equation, Eq.(13b), that is, $\nabla \cdot \mathbf{u}^{(*)} \neq 0$. Satisfaction of the continuity equation may be accomplished by updating the velocity field $\mathbf{u}^{(*)}$ with a velocity correction field $\delta \mathbf{u}^{(\kappa+1)}$ as:

$$\mathbf{u}^{(\kappa+1)} = \mathbf{u}^{(*)} + \delta \mathbf{u}^{(\kappa+1)}. \tag{20}$$

Furthermore, assuming the velocity correction field to be irrotational, i.e. $\nabla \times \delta \mathbf{u}^{(\kappa+1)} = 0$, a Helmholtz potential (or correction potential) $\phi^{(\kappa+1)}$ can be defined

as: $\nabla\phi^{(\kappa+1)} \equiv -\delta\mathbf{u}^{(\kappa+1)}$. Now, if the new velocity update is required to satisfy the continuity equation, i.e. $\nabla\cdot\mathbf{u}^{(\kappa+1)} = 0$, a relationship for the correction-potential $\phi^{(\kappa+1)}$ can be expressed in the form of a Poisson equation as:

$$\nabla^2\phi^{(\kappa+1)} = \nabla\cdot\mathbf{u}^{(*)}. \tag{21}$$

This Poisson equation for the Helmholtz potential can be solved by imposing a proper and complete set of boundary conditions, generalized as:

$$\beta\frac{\partial\phi^{(\kappa+1)}}{\partial n} + \gamma\phi^{(\kappa+1)} = \sigma, \tag{22}$$

where β and γ are variables defined at each problem .

Once the Helmholtz-Poisson problem is solved, the velocity field is updated and forced to satisfy continuity. From the estimated velocity field $\mathbf{u}^{(\kappa+1)}$ the vorticity values can be calculated from equation (14) over all the spatial domain Ω. Thus, the vorticity transport equation (17) is now solvable using the new vorticity boundary values. The updated vorticity values $\omega^{(\kappa+1)}$ are used for the next iteration. The convergence of the velocity and vorticity components are monitored in each iteration, e.g. $\left|u_i^{k+1} - u_i^k\right| \leq 10^{-6}$, as is the satisfaction of the continuity equation, e.g. $\frac{\partial u^{(\kappa+1)}}{\partial x} + \frac{\partial v^{(\kappa+1)}}{\partial y} \leq 10^{-6}$. As soon as both the prescribed convergence criteria are satisfied, the iterative procedure is ended otherwise the old vorticity values are replaced by the new ones and the aforementioned procedure is repeated. Regarding the boundary conditions one gets:

(A) Boundary conditions for the velocity components, u and v:

1. Wall: $u = 0$ and $v = 0$,
2. Inlet: $u = \widehat{u}$ and $v = \widehat{v}$,
3. Outlet: $\frac{\partial u^{(\kappa+1)}}{\partial\mathbf{n}} = -\frac{\partial v^{(\kappa)}}{\partial y}\mathbf{n}_x + \frac{\partial u^{(\kappa)}}{\partial y}\mathbf{n}_y$ and

$$\frac{\partial v^{(\kappa+1)}}{\partial\mathbf{n}} = -\frac{\partial u^{(\kappa)}}{\partial x}\mathbf{n}_y + \frac{\partial v^{(\kappa)}}{\partial x}\mathbf{n}_x.$$

(B) Boundary conditions for the Helmholtz potential,ϕ:

1. Wall: $\frac{\partial\phi}{\partial\mathbf{n}} = 0$,
2. Inlet: $\frac{\partial\phi}{\partial\mathbf{n}} = 0$,
3. Outlet: $\phi = 0$,

where the notation $\widehat{\mathbf{u}}$ signifies prescribed values of u, for instance, and $\frac{\partial u}{\partial\mathbf{n}}$ denotes derivative with respect to the outward-drawn normal to the corresponding surface, $\widehat{\mathbf{n}}$. The latter has components, $\mathbf{n}_x$ and $\mathbf{n}_y$, respectively.

4 Numerical results

In this section we present the numerical results obtained using the proposed numerical scheme for three representative problems, that is, the square lid-driven cavity flow, flow over a backward-facing step, and an irregular geometry describing a stenosed 2D blood vessel.

4.1 Lid-Driven cavity flow

The flow in closed cavities mechanically driven by tangentially moving walls represents a basic problem in fluid mechanics. In this case, geometry description is a simple task, however, computation is not necessarily so, even in the laminar regime as, for example, corner eddies have to be captured and the singularities have to be taken care off. In the classical configuration one of the side walls are moving either steadily or in a time-dependent manner tangentially to itself (one sided lid-driven cavity). The domain of the problem, without loosing generality, is $[0,1] \times [0,1]$ as shown in Fig. 1.

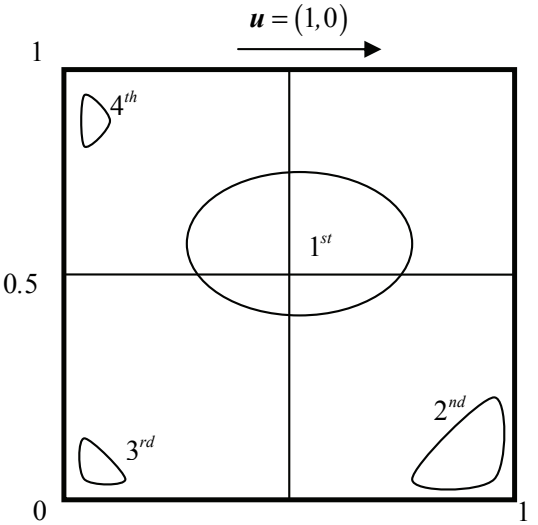

Figure 1: The lid-driven cavity flow.

The velocity $\mathbf{u} = (1,0)$ is assigned on the top-boundary, while no-slip boundary conditions are assigned for the remaining boundaries. The no-slip boundary condition on the wall motivates the interior viscous flow. The nodal distribution is a regular one. The results are compared with those obtained in [Ghia, Ghia and Shin

(1982)], where the multigrid finite difference method was used, with a mesh size of 257×257. In order to calculate the streamfunction values, the boundary conditions for the driven cavity are given by:

$\psi = 0, \quad \frac{\partial \psi}{\partial x} = 0$ on $x = 0$ and $x = 1$.

$\psi = 0, \quad \frac{\partial \psi}{\partial y} = 0$ on $y = 0$.

$\psi = 0, \quad \frac{\partial \psi}{\partial y} = 1$ on $y = 1$.

The Reynolds numbers used for the present study are

$$\{100, 400, 1000, 3200, 5000, 7500, 10000\}.$$

During the numerical experiments, we observed that the proposed algorithm converges in about 1000 iterations. Compared to the large mesh used in [Ghia, Ghia and Shin (1982)], it was found that the MLS approximations systematically provide results of comparable accuracy even with coarse grids, especially for moderate Reynolds numbers ($Re < 1000$). More precisely, for Reynolds numbers up to $Re = 3200$, a grid of 161×161 was used and reported here, while for higher values a regular grid of 321×161 was utilized.

The u-velocity on the vertical center line $x = 0.5$ and the v-velocity on the horizontal center line $y = 0.5$ are given in Figures 2 and 3, respectively.

It is shown that all the results obtained from the current meshfree point collocation method are in good agreement with the data by Ghia [Ghia, Ghia and Shin (1982)], which is a widely accepted reference for validation. Furthermore, we present a table for three vortices taking place in the cavity flow as the Reynolds number increases. In Table 1 the strengths and positions of the primary, secondary and ternary vortexes, denoted by 1st, 2^{nd}, 3^{rd} and 4^{th}in Fig. 1, are listed. The numerical results are in very good agreement with the results obtained by several authors [Hou, Zou, Chen, Doolen and Cogley (1995), Gupta and Kalita (2005), Erturk, Corke and Cokcol (2005)]. The streamlines and vorticity contours are illustrated in Fig. 4.

4.2 Backward-facing step flow

The next benchmark problem presented is flow over the backward-facing step. The problem of fluid flow over a backward-facing step has been studied extensively in the last three decades [Armaly, Durst, Pereira and Schonung (1983), Gartling (1990)], due to the complex physics encountered. Herein, the problem is investigated numerically using the meshless point collocation method. The Navier-Stokes equations were solved using the velocity-vorticity formulation.

Consider a channel of width L downstream of the origin, and of width $L/2$ upstream

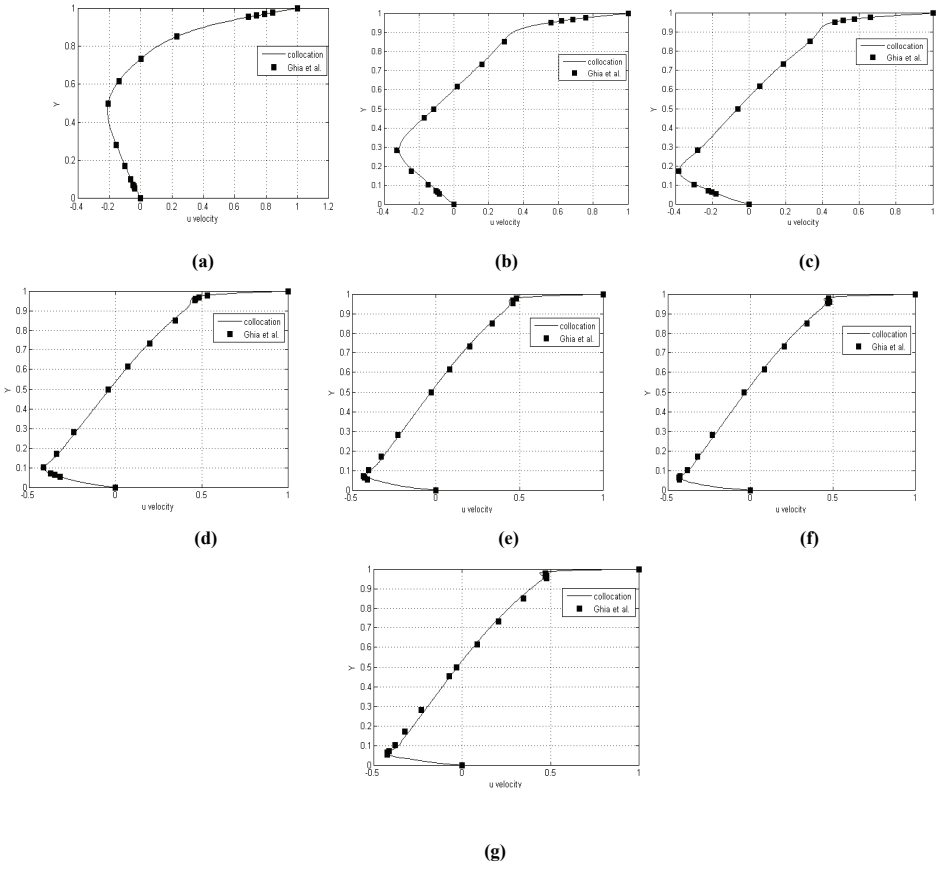

Figure 2: The u-velocity on the vertical section $x = 0.5$of the square lid-driven cavity problem for **(a)** $Re = 100$ **(b)** $Re = 400$ **(c)** $Re = 1000$ **(d)** $Re = 3200$ **(e)** $Re = 5000$ **(f)** $Re = 7500$ and **(g)** $Re = 10000$. Results of Ghia et al. are compared with the current numerical solutions.

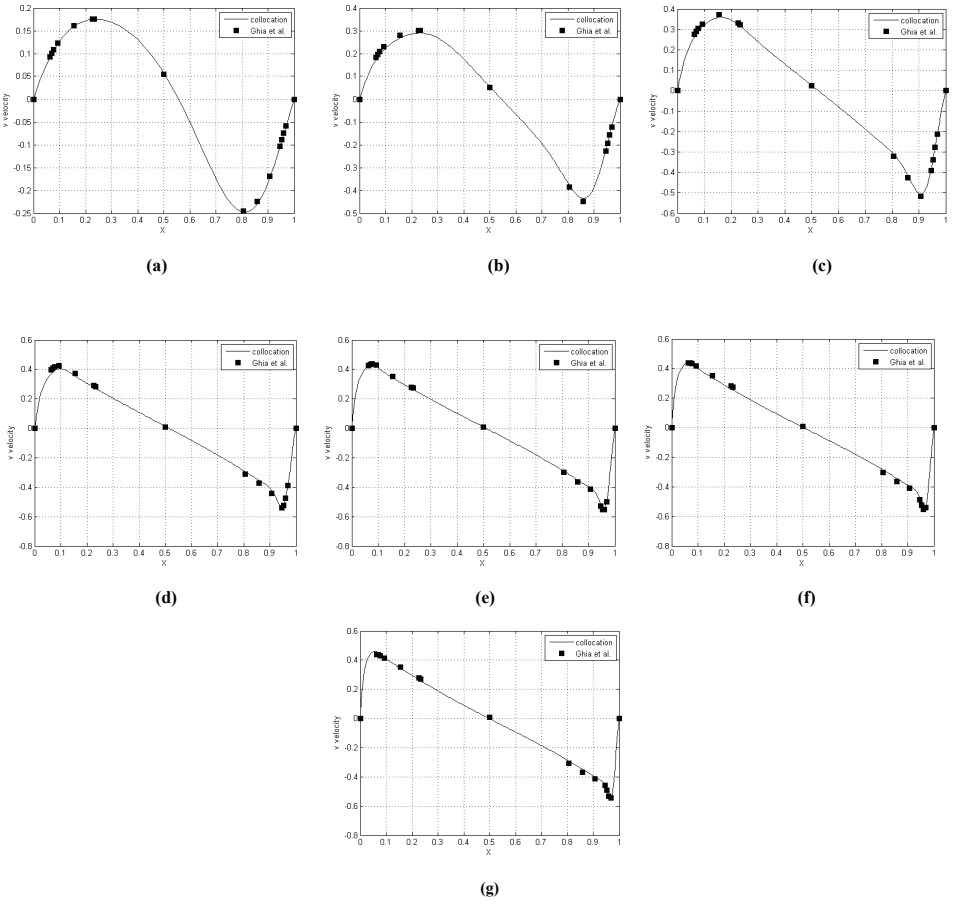

Figure 3: The v-velocity on the horizontal section $y = 0.5$ of the square lid-driven cavity problem for **(a)** $Re = 100$ **(b)** $Re = 400$ **(c)** $Re = 1000$ **(d)** $Re = 3200$ **(e)** $Re = 5000$ **(f)** $Re = 7500$ and **(g)** $Re = 10000$. Results of Ghia et al. are compared with the current numerical solutions.

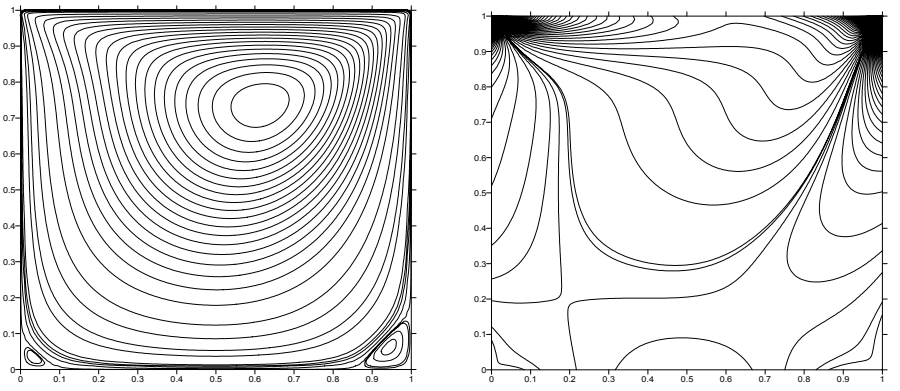

(a)

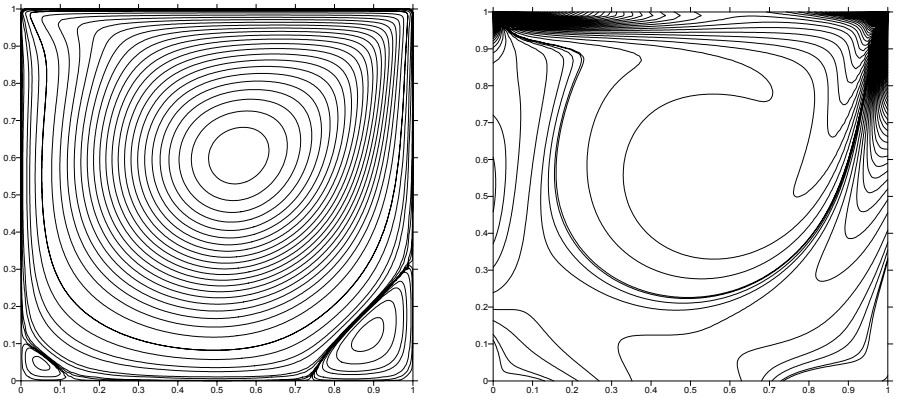

(b)

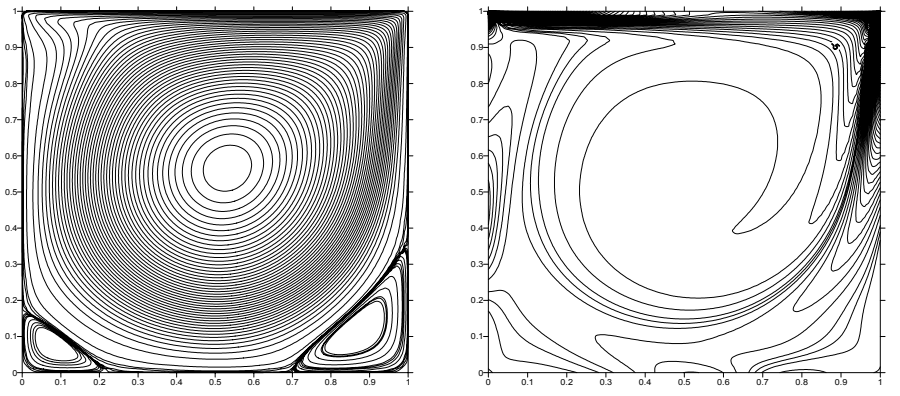

(c)

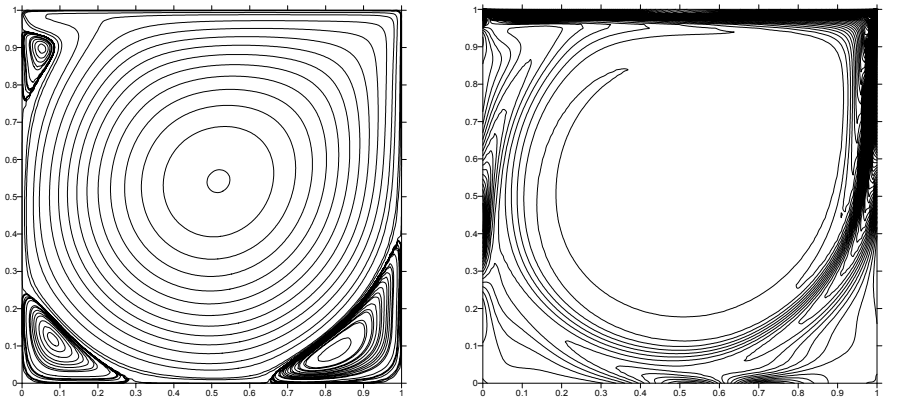

(d)

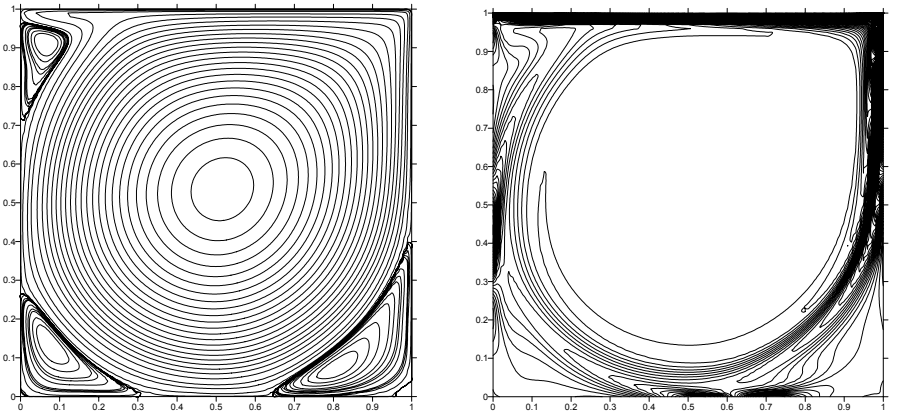

(e)

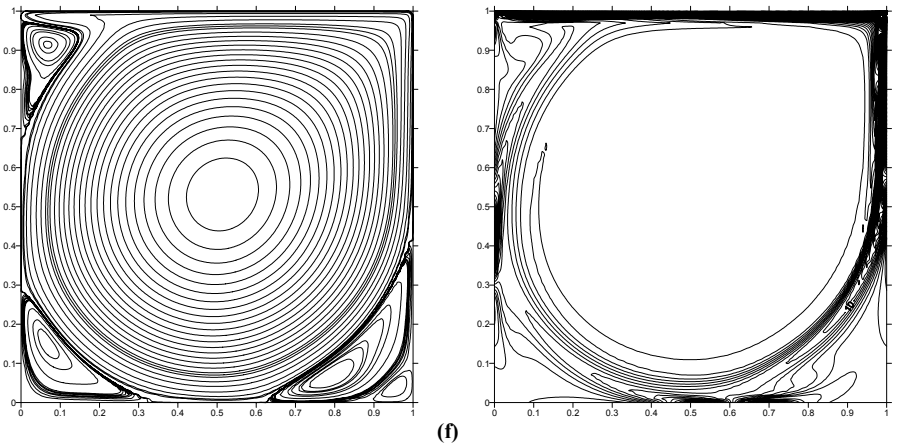

(f)

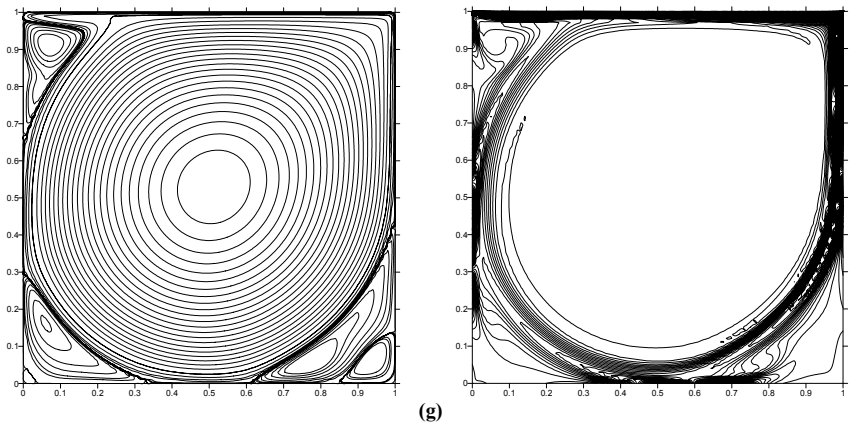

(g)

Figure 4: Streamlines (left) and vorticity (right) contours for the lid-driven cavity flow for **(a)** $Re = 100$ **(b)** $Re = 400$ **(c)** $Re = 1000$ **(d)** $Re = 3200$ **(e)** $Re = 5000$ **(f)** $Re = 7500$ and **(e)** $Re = 10000$.

of the origin, separated by a backward-facing step. Flow is assumed to be fully developed as it passes through the inlet at $x = 0$, and has an average velocity $\widetilde{U}$. The problem domain is the channel starting at the inlet and extending downstream a distance D, long enough for the flow to become again fully developed. The Reynolds number is defined as $\widetilde{U}L/v$. The boundary conditions for the problem are given in Table 3. The downstream distance D is taken to be $30L$, in order for the flow to be fully developed.

Contours of the streamfunction and vorticity for $Re = 200$ are presented in Figure 6. A recirculation zone is noticeably formed downstream the top face. The recirculation zone details obtained by the present method are compared with those obtained by using global Radial Basis Functions (RBF) [Chinchapatnam, Djidjeli and Nair (2007)] and the $h-p$finite elements [Barragy (1993)]. The numerical results obtained regarding the length of the recirculation and the value of $\psi_{\min}$ are in fair agreement with the FEM, as shown in Table 4.

The behavior under higher Reynolds numbers was examined. Authors in [Armaly, Durst, Pereira and Schonung (1983)] measured separation and re-attachment points for a wide range of Reynolds numbers including the case of $Re = 800$. Unfortunately, three-dimensional effects in the channel appear to be significant for $Re > 400$, making comparisons with two-dimensional simulations less than satisfactory. However, the flow statistics listed in the Tables 5 and 6 can, with some caution, be compared with results from other experimental and numerical inves-

Table 1: Comparison of centre of primary, secondary (right down corner), and third (left down corner) vortices, and the corresponding streamfunction values.

Re	Reference	$\psi_{\min}$	(x_{1st}, y_{1st})	$\psi_{\max}$	(x_{2nd}, y_{2nd})	$\psi_{\min}$	(x_{3rd}, y_{3rd})
100	Ghia et al.	-0.1034	(0.6172, 0.7344)	1.25e-5	(0.9453, 0.0625)	1.75e-6	(0.0313, 0.0391)
	Hou et al.	-0.1030	(0.6196, 0.7373)	1.22e-5	(0.9451, 0.0627)	1.72e-6	(0.0392, 0.0353)
	Gupta et al.	-0.1030	(0.6125, 0.7375)	1.45e-5	(0.9375, 0.0625)	1.83e-6	(0.0375, 0.0375)
	Sanyasiraju et al.	-0.1013	(0.6357, 0.7500)	4.38e-5	(0.9333, 0.0667)	N/A	N/A
	Kim et al.	-0.1030	(0.6134, 0.7375)	1.22e-5	(0.9396, 0.0625)	1.72e-6	(0.0350, 0.0354)
	present (MPC)	-0.1030	(0.6155, 0.7355)	1.25e-5	(0.9375, 0.0610)		
400	Ghia et al.	-0.114	(0.5547, 0.6055)	6.42e-4	(0.8906, 0.1250)	1.42e-5	(0.0508, 0.0469)
	Hou et al.	-0.112	(0.5608, 0.6078)	6.19e-4	(0.8902, 0.1255)	1.30e-5	(0.0549, 0.0510)
	Gupta et al.	-0.113	(0.5500, 0.6125)	6.48e-4	(0.8875, 0.1250)	1.30e-5	(0.0500, 0.0500)
	Sanyasiraju et al.	N/A	N/A	N/A	N/A	N/A	N/A
	Kim et al.	-0.114	(0.5525, 0.6100)	5.87e-4	(0.8873, 0.1250)	7.37e-6	(0.0500, 0.0375)
	present (MPC)	-0.114	(0.5540, 0.6062)	6.44e-4	(0.8912, 0.1250)	1.41e-5	(0.0518, 0.0467)
1000	Ghia et al.	-0.1179	(0.5313, 0.5625)	1.75e-3	(0.8594, 0.1094)	2.31e-4	(0.0859, 0.0781)
	Hou et al.	-0.1180	(0.5333, 0.5647)	1.69e-3	(0.8667, 0.1137)	2.22e-4	(0.0902, 0.0784)
	Gupta et al.	-0.1170	(0.5250, 0.5625)	1.70e-3	(0.8625, 0.1125)	2.02e-4	(0.0875, 0.0750)
	Sanyasiraju et al.	-0.1164	(0.5305, 0.5601)	1.96e-3	(0.8651, 0.1118)	N/A	N/A
	Kim et al.	-0.1220	(0.5311, 0.5714)	1.40e-3	(0.8624, 0.1127)	1.24e-4	(0.0803, 0.0732)
	present (MPC)	-0.1200	(0.5328,0.5754)	1.94e-3	(0.8528, 0.1071)	2.30e-4	(0.0879, 0.0784)
3200	Ghia et al.	-0.1204	(0.5165,0.5469)	3.14e-03	(0.8125,0.0859)	9.78e-04	(0.0859,0.1094)
	Sanyasiraju et al.	-0.1155	(0.5154,0.5305)	3.00e-03	()0.8310,0.0844	1.13e-03	(0.0844,0.1118)
	present (MPC)	-0.1202	(0.5153,0.5357)	3.11e-03	(0.8235,0.0861)	9.72e-04	(0.0852,0.1102)
5000	Ghia et al.	-0.1189	(0.5117,0.5352)	3.08e-03	(0.8086,0.0742)	1.36e-03	(0.0703,0.1367)
	Erturk	- 0.1213	(0.5150,0.5350)	3.06e-03	(0.8050,0.0733)	1.36e-03	(0.0733,0.1367)
	present (MPC)	- 0.1212	(0.5140,0.5350)	3.06e-03	(0.8070,0.0743)	1.36e-03	(0.0753,0.1372)
7500	Ghia et al.	-0.1199	(0.5117,0.5322)	3.30e-03	(0.7813,0.0625)	1.47e-03	(0.0645,0.1504)
	Erturk	-0.1209	(0.5133,0.5317)	3.21e-03	(0.7900,0.0650)	1.52e-03	(0.0650,0.1517)
	present (MPC)	-0.1183	(0.5156,0.5345)	3.36e-03	(0.7900,0.0700)	1.47e-03	(0.0655,0.1524)
10000	Ghia et al.	-0.1197	(0.5117,0.5333)	3.42e-03	(0.7656,0.0586)	1.52e-03	(0.0586,0.1641)
	Erturk	-0.1204	(0.5117,0.5300)	3.17e-03	(0.7767,0.0600)	1.59e-03	(0.0583,0.1633)
	present (MPC)	-0.1224	(0.5127,0.5330)	3.27e-03	(0.7867,0.0652)	1.62e-03	(0.0593,0.1663)

tigations [Gartling (1990)]. Furthermore, contours of the streamfunction and the vorticity are presented in Figures 7 and 8. A regular grid of 121x31 nodes was used for the present work.

4.3 Blood flow through vascular stenosis

The effect of constrictions in two-dimensional tubes has many important applications, especially in biofluids. The partial occlusion of arteries due to stenotic obstruction is one of the most frequent abnormalities in blood circulation. Artery stenosis afflicts patients with atherosclerotic disease and leads to vascular malper-

Table 2: Comparison of centre of top left secondary vortex and the corresponding stream function.

Re	Reference	ψ	(x_{4th}, y_{4th})
3200	Ghia et al.	7.28e-04	(0.0547,0.8984)
	Sanyasiraju et al.	6.87e-04	(0.0555,0.8954)
	present (MPC)	7.08e-04	(0.0542,0.8974)
5000	Ghia et al.	1.46e-03	(0.0625,0.9102)
	Erturk	1.44e-03	(0.0633,0.9100)
	present (MPC)	1.44e-03	(0.0643,0.9120)
7500	Ghia et al.	2.05e-03	(0.0664,0.9141)
	Erturk	2.11e-03	(0.0667,0.9133)
	present (MPC)	2.11e-03	(0.0666,0.9134)
10000	Ghia et al.	2.42e-03	(0.0703,0.9141)
	Erturk	2.59e-03	(0.0717,0.9117)
	present (MPC)	2.60e-03	(0.0727,0.9137)

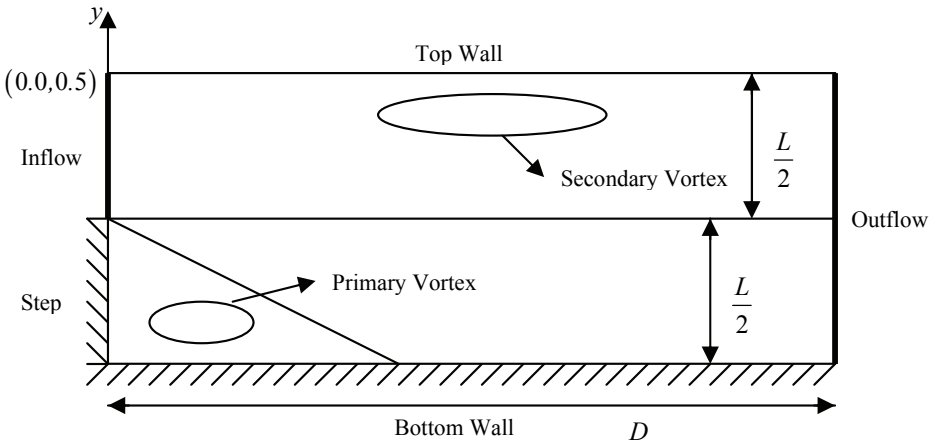

Figure 5: Backward-facing step flow.

Table 3: Boundary conditions for backward-facing step.

Inlet	$\psi = 2y^2(3-4y)$	$\partial\psi/\partial x = 0$
Outlet	$\psi = (1/4)\left(1+3y-4y^3\right)$	$\partial\psi/\partial x = 0$
Step	$\psi = 0$	$\partial\psi/\partial x = 0$
Bottom wall	$\psi = 0$	$\partial\psi/\partial y = 0$
Top wall	$\psi = 0.5$	$\partial\psi/\partial y = 0$

Table 4: Backward-facing step:$Re = 200$, primary vortex strength and location, length of recirculation region and its comparison with higher-order finite elements.

	$h-p$finite elements	RBF	MPC
Length of recirculation	2.67	2.72	2.64
$\psi_{\min}$	-0.0331	-0.0315	-0.0331
$\psi_{\min}$ location	(1.0021,-0.2030)	(1.333,-0.2167)	(1.0001,-0.2000)

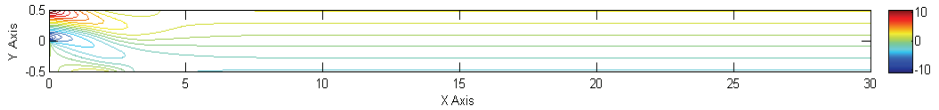

(a)

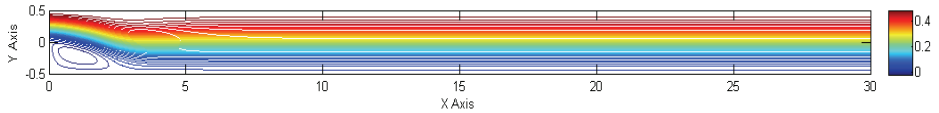

(b)

Figure 6: **(a)** Vorticity contours and **(b)** streamfunction contours for $Re = 200$.

fusion. Stenosis is typically caused by ostial plaque formation with an eventual occlusion and is currently considered to be an independent predictor of death regardless of the extent and severity of systemic atherosclerosis. For the aforementioned reasons, the results of a steady flow analysis for this situation is an important first step in studying the effects of arterial stenosis on the human body. It is well known that, once such obstruction is formed, the blood flow is significantly altered and fluid dynamic factors play an important role as the stenosis continues to develop.

In the present study, a 2D vascular model with single constriction (occlusion) has

Table 5: Lower wall eddy. Mesh configurations **A**, **B**, **C**, **D** and **E** are described in [Gartling (1990)].

Mesh	**Vortex centre** (x,y)	**Stream function** ψ **at vortex centre**	**Vorticity** ω **at vortex centre**	**Length of recirculation zone**
A	(3.000, -0.167)	-0.0335	-2.518	5.81
B	(3.300, -0.200)	-0.0342	-2.249	6.07
C	(3.350, -0.200)	-0.0342	-2.285	6.09
D	(3.350, -0.200)	-0.0342	-2.283	6.10
E	(3.350, -0.200)	-0.0342	-2.283	6.10
present	(3.403, -0.203)	-0.0332	-2.364	6.02

Table 6: Upper wall eddy. Mesh configurations **A**, **B**, **C**, **D** and **E** are described in [Gartling (1990)].

Mesh	**Vortex centre** (x,y)	**Stream function** ψ **at vortex centre**	**Vorticity** ω **at vortex centre**	**Length of recirculation zone**
A	(7.500, 0.333)	0.5071	0.959	5.69
B	(7.400, 0.300)	0.5064	1.319	5.64
C	(7.400, 0.300)	0.5064	1.321	5.63
D	(7.400, 0.300)	0.5064	1.324	5.63
E	(7.500, 0.300)	0.5064	1.322	5.63
present	(7.450, 0.300)	0.5096	1.283	5.66

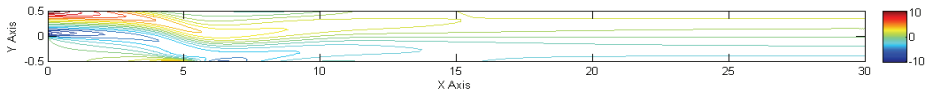

(a)

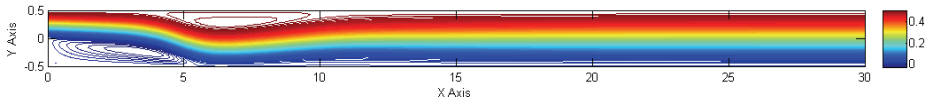

(b)

Figure 7: **(a)** Vorticity contours and **(b)** streamfunction contours for $Re = 800$.

been considered, as shown in Figure 8. A parabolic velocity profile $u = y - y^2$,

$v = 0$ was considered at inflow and outflow boundary conditions, considering a fully developed flow. An ellipse was used to describe the stenosis and the percentage reduction in diameter of the tube. Due to the sudden reduction of the diameter at the constriction region of the tube, the numerical schemes loose stability and tend to diverge. Herein, the velocity-correction method ensures the continuity equation is satisfied, leading to both convergence and stability of the proposed scheme. The computations are carried out for various Reynolds numbers and steady-state solutions have been obtained. The results have been compared with the results obtained using the well-established, commercial CFD package ANSYS CFX.

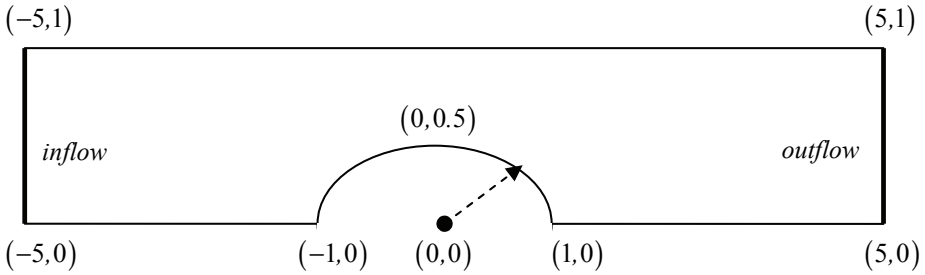

Figure 8: Vascular geometry with stenosis defined as $x^2 + 4y^2 = 1$.

The distribution of the nodes considered for the computations was of the so-called Type-I [Kim and Liu (2006)], embedded in the prescribed geometry, shown in Figure 9 (a) [Bourantas, Skouras and Nikiforidis (2009)]. The Type-I nodal distribution ensures the convergence of the discrete harmonic operator used. Additionally, a non-uniform distribution of the nodes was also considered. The total number of nodes for the case of $Re = 800$ is 4096.

The velocity magnitude comparison is provided in Figure 10, as obtained by the MPC and the FVM solvers. The velocity magnitude contours demonstrate a very good qualitative agreement between the values predicted by the FVM and the MPC solvers. Particularly, the MPC method captures the vortex formatting behind the obstacle, consistently with the FVM. For comparison reasons, the plots of the u velocity component obtained by the proposed scheme and the ANSYS CFX 12.0 are presented in Figure 11.

To validate quantatively the accuracy of the meshless method, we further focus on and plot the meshless and the FVM u-velocity profiles at three vertical sections just before, right at, and just after the obstacle. The locations of the u-velocity profiles are defined as $X_1\,(x = -2)$, $X_2\,(x = 0)$ and $X_3\,(x = 2)$. Although some minor discrepancies are evident, the velocity profiles indicate a high level of quantita-

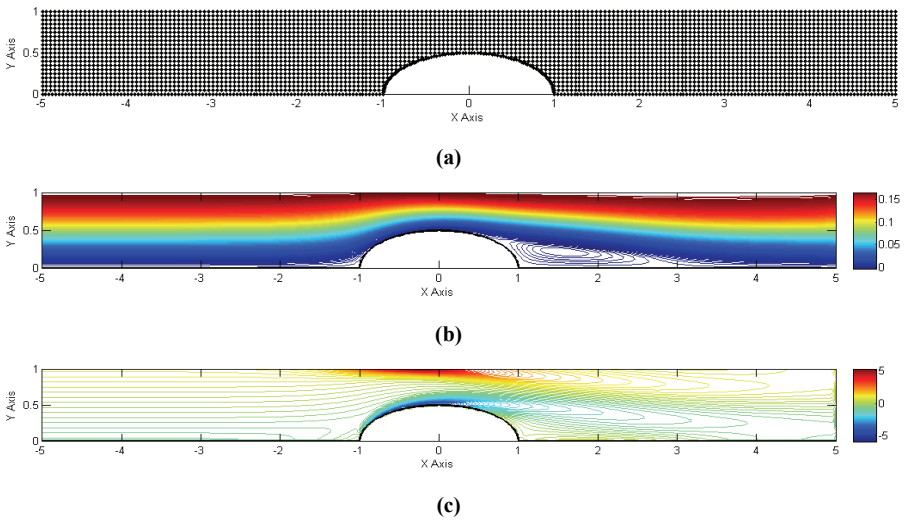

Figure 9: **(a)** Embedded Type-I nodal distribution **(b)** streamline contours and **(c)** vorticity contours for $Re = 800$.

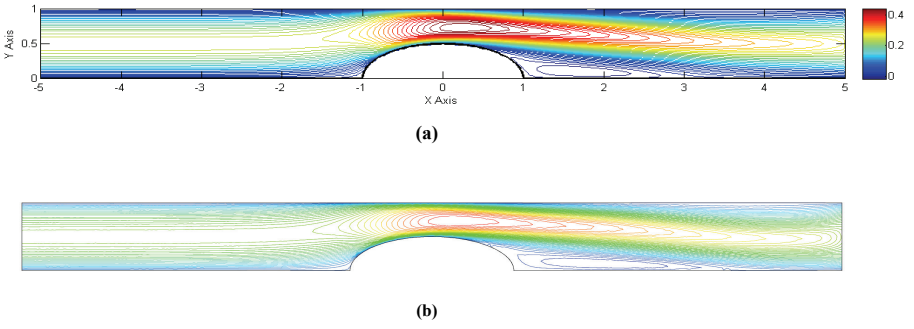

Figure 10: u-velocity contours for $Re = 800$ using **(a)** MPC method and **(b)** conventional FVM solvers (ANSYS CFX).

tive agreement between the meshless method and the FVM. The agreement of the meshless point collocation method with the FVM is notable.

In order to demonstrate the applicability of the MPC method at flows in elevated Reynolds numbers, a case with $Re = 1600$ was considered, Figure 12. The outflow boundary is now shifted at $x = 10$ for the flow to be fully developed.

Finally, depicting the applicability of the proposed numerical scheme, we used an

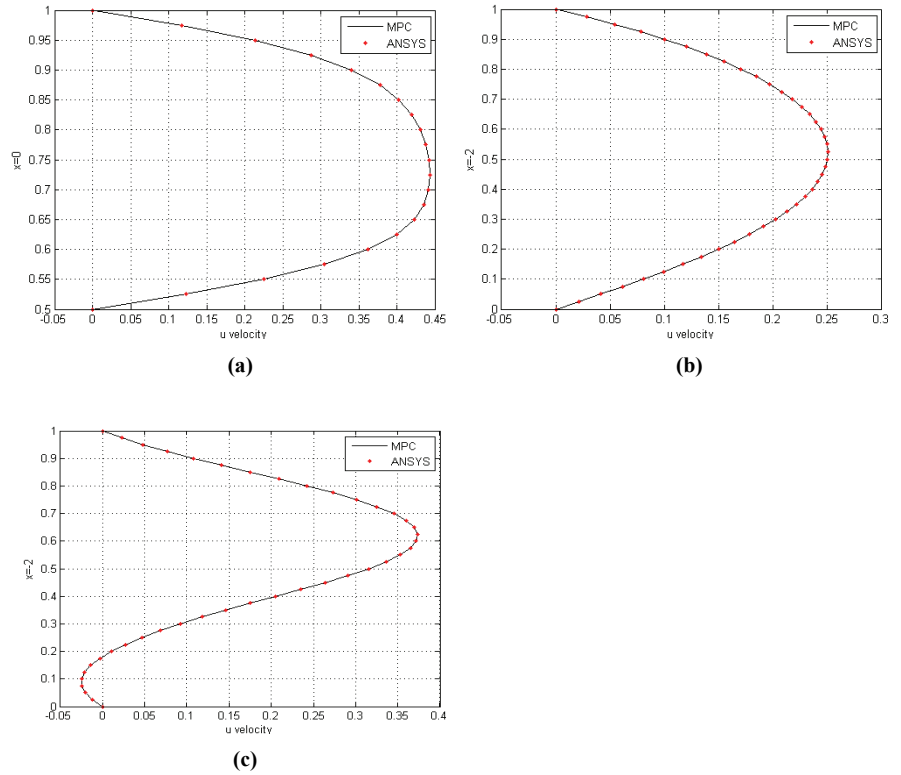

Figure 11: u-velocity profiles at three vertical sections **(a)** $x = 0$ **(b)** $x = -2$ and **(c)** $x = 2$ with the proposed MPC and ANSYS CFX.

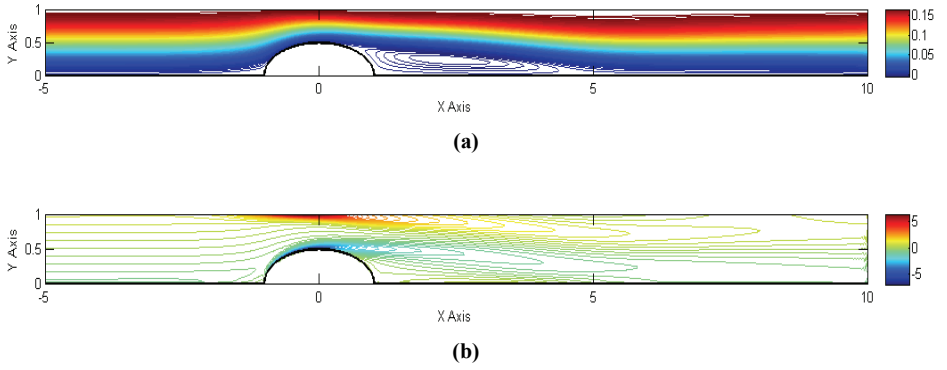

Figure 12: **(a)** Streamline contours and **(b)** vorticity contours for $Re = 1600$.

irregular nodal distribution as shown in Fig. 13. The results obtained are in a very good agreement with those of the regular, Type-I embedded nodal distribution and ANSYS CFX.

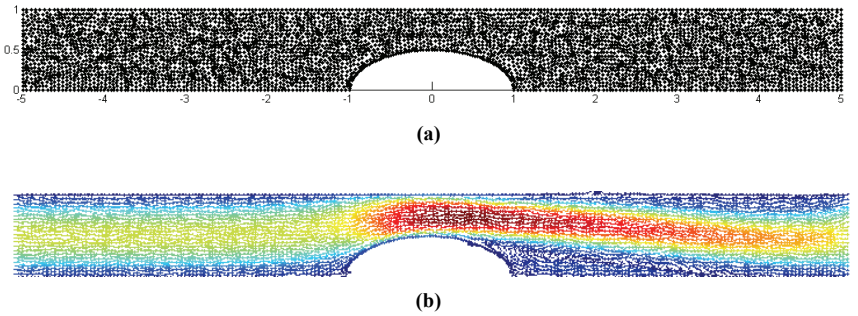

Figure 13: **(a)** Irregular nodal distribution and **(b)** velocity arrows for $Re = 800$.

5 Conclusions

A meshless, point collocation method with MLS approximation is presented for the numerical solution of the incompressible Navier-Stokes equations using the velocity-vorticity formulation. A velocity correction technique is applied, ensuring the conformity of the continuity equation. The proposed method, being truly meshless, avoids the time-consuming meshing and mesh adapting procedures of traditional FEM and FVM methods altogether, while the application of specific nodal distributions ensure accuracy and convergence at typical resolutions. The method obtains numerical solutions using either uniform or non-uniform nodal distributions for a wide range of Reynolds number (up to 10000). The numerical solutions of three benchmark problems were compared with previous works with excellent agreement. The results of the MPC method were also compared with the ones derived from the commercial Computational Fluid Dynamics package ANSYS CFX for the irregular geometry, where the accuracy of the method at medium resolutions was also evident. The MPC method with the velocity-correction technique can be straightforwardly extended to three-dimensional complex geometries for steady state and transient flow problems.

References

Ahn, M. Y.; Chang, K. S.; Choe, H. J.; Kim, Y. S. (2006); Analysis of a meshfree method for the compressible Euler equations, *Journal of the Korean Mathematical Society*, vol. 43, pp. 1081-1098.

Aluru, N. R. (2000): A point collocation method based on reproducing kernel approximations. *International Journal for Numerical Methods in Engineering*, vol. 47, pp. 1083 –1121.

Arnold, D. N.; Liu X. (1995): Local error estimates for finite element discretizations of the Stokes equations, *Mathematical Modelling and Numerical Anaysis.*, vol. 29, pp. 367–389.

Armaly, B. F.; Durst, F.; Pereira, J. C. F.; Schonung, B. (1983): Experimental and theoretical investigation of backward-facing step flow. *Journal of Fluid Mechanics*, vol. 127, pp. 473–496.

Arefmanesh, A.; Najafi, M.; Abdi, H. (2008): Meshless Local Petrov-Galerkin Method with Unity Test Function for Non-Isothermal Fluid Flow. *CMES: Computer Modeling in Engineering and Sciences*, vol. 25, pp. 9-22.

Atluri, S. N.; Kim, H. G.; Cho, J. Y. (1999): A critical assessment of the truly Meshless local Petrov–Galerkin (MLPG) methods. *Computational Mechanics*, vol. 24, pp. 348–372.

Atluri, S. N.; Shen, S. P. (2002): *The Meshless Local Petrov–Galerkin (MLPG) Method*, 440 pages, Tech Science Press, Encino USA.

Barragy, E. (1993): Parallel finite element methods and iterative solution techniques for viscous incompressible flows. *PhD thesis,*University of Texas at Austin.

Baez, E.; Nicolas, A. (2009): Recirculation of viscous incompressible flows in enclosures. *CMES: Computer Modeling in Engineering and Sciences*, vol. 41, pp. 107-130.

Babuska, I. (1973): The finite element method with Lagrange multipliers. *Numerische Mathematik*, vol. 20, pp. 179-192.

Babuska, I. (1971): Error bounds for finite element method. *Numerische Mathematik*, vol. 16, pp. 322-333.

Belytschko, T.; Lu, Y. Y.; Gu, L. (1994): Element free Galerkin methods. *International Journal for Numerical Methods in Engineering*, vol. 37, pp. 229-256.

Bourantas, G. C.; Skouras, E. D.; Nikiforidis, G. C. (2009): Adaptive support domain implementation on the moving least squares approximation for Mfree methods applied on elliptic and parabolic PDE problems using strong-form description, *CMES: Computer Modeling in Engineering and Sciences*, vol. 43, pp. 1-25.

Brezzi, F. (1974): On the existence, uniqueness and, approximation of saddle-point problems arising from Lagrange multipliers. *RAIRO Analysis of Numerical Mathematics*, vol. 53, pp. 225-235.

Chinchapatnam, P. P.; Djidjeli, K.; Nair, P. B. (2007): Radial basis function

meshless method for the steady incompressible Navier- Stokes equations. *International Journal of Computer Mathematics,* vol. 84, pp. 1509–1526.

Choe, H. J.; Kim, D. W.; Kim, H. H.; Kim, Y. S. (2001): Meshless method for the stationary incompressible Navier–Stokes equations. *Discrete and Continuous Dynamical Systems-Series B*, vol. 1, pp. 495–526.

Divo, E.; Kassab, A. (2006): Iterative domain decomposition meshless method modeling of incompressible viscous flows and conjugate heat transfer. *Engineering Analysis with Boundary Elements*, vol. 30, pp. 465–478.

Duarte, C. A.; Oden, J. T. (1996): An h-p adaptive method using clouds. *Computer Methods in Applied Mechanics and Engineering*, vol. 139, pp. 237–262.

Erturk, E.; Corke, T. C.; Cokcol C. (2005): Numerical solutions of 2-D steady incompressible driven cavity flow at high Reynolds numbers. *International Journal for Numerical Methods in Fluids*, vol. 48, pp. 747–774.

Gartling, D. K. (1990): A test problem for outflow boundary conditions-flow over a backward-facing step. *International Journal for Numerical Methods in Fluids*, vol. 11, pp. 953-967.

Ghia, U.; Ghia, K. N.; Shin, C. T. (1982): High-Re solutions for incompressible flow using the Navier-Stokes equations and a multigrid method. *Journal of Computational Physics*, vol. 48, pp. 387-411.

Gingold, R. A.; Monaghan, J. J. (1977): Smoothed particle hydrodynamics: theory and application to non-spherical stars. *Monthly Notices of the Royal Astronomical Society*, vol. 181, pp. 275–389.

Grimaldi, A.; Pascazio, G.; Napolitano M. (2006): A Parallel Multi-block Method for the Unsteady Vorticity-velocity Equations. *CMES: Computer Modeling in Engineering and Sciences*, vol. 14, pp. 45-56.

Gunther, F.; Liw, W. K.; Diachin, D. (2000): Multi-scale meshfree parallel computations for viscous, compressible flows. *Computer Methods in Applied Mechanics and Engineering*, vol. 190, pp. 279–303.

Gupta, M. M.; Kalita, J. C. (2005): A new paradigm for solving Navier-Stokes equations: streamfunction-velocity formulation. *Journal of Computational Physics*, vol. 207, pp. 52-68.

Harlow, F. H.; Welch, J. E. (1965): Numerical calculation of time dependent viscous incompressible flow of fluids with a free surface. *Physics of Fluids*, vol. 8, pp. 2182–9.

Hou, S.; Zou, Q.; Chen, S.; Doolen, G.; Cogley, A. (1995): Simulation of cavity flows by the lattice Boltzmann method. *Journal of Computational Physics*. vol. 118, pp. 329-347.

Kim, D. W.; Liu, W. K. (2006): Maximum principle and convergence analysis for the meshfree point collocation method. *SIAM Journal on Numerical Analysis,* vol. 44, pp. 515–539.

Kim, Y.; Kim, D. W.; Jun, S.; Lee, J. H. (2007): Meshfree point collocation method for the stream-vorticity formulation of 2D incompressible Navier-Stokes equations. *Computer Methods in Applied Mechanics and Engineering*, vol. 196, pp. 3095-3109.

Kim, Y.; Kim, D. W.; Jun, S.; Lee, J. H. (2007): Meshfree point collocation method for the stream-vorticity formulation of 2D incompressible Navier-Stokes equations. *Computer Methods in Applied Mechanics and Engineering,* vol. 196, pp. 3095-3109.

Kosec, G.; Sarler, B. (2008): Local RBF Collocation Method for Darcy Flow. *CMES: Computer Modeling in Engineering and Sciences*, vol. 25, pp. 197-207.

Ligget, J. A. (1994): *Fluid Mechanics*, McGraw-Hill: New-York.

Lin, H.; Atluri, S. N. (2001): The Meshless Local Petrov-Galerkin (MLPG) Method for Solving Incompressible Navier-Stokes Equations. *CMES: Computer Modeling in Engineering and Sciences*, vol. 2, pp.117-142.

Liu, G. R. (2002): *Mesh Free Methods, Moving beyond the Finite Element Method*, CRC Press.

Liu, W. K.; Jun, S.; Zhang, Y. F. (1995): Reproducing kernel particle methods. *International Journal for Numerical Methods in Fluids*, vol. 20, pp. 1081–1106.

Liu, W. K.; Jun, S.; Li, S.; Adee, J.; Belytschko, T. (1995): Reproducing kernel particle methods for structural dynamics. *International Journal for Numerical Methods in Engineering*, vol. 38, pp. 1655 –1679.

Liu, W. K.; Li, S.; Belytschko, T. (1996): Moving least square reproducing kernel methods (I) methodology and convergence. *Computer Methods in Applied Mechanics and Engineering*, vol. 143, pp. 422– 433.

Liu, W. K.; Jun, S.; Sihling, D. T.; Chen, Y.; Hao, W. (1997): Multiresolution reproducing kernel particle method for computational fluid dynamics. *International Journal for Numerical Methods in Fluids*, vol. 24, pp. 1391–1415.

Mai-Duy, N.; Tran-Cong T. (2001): Numerical solution of differential equations using multiduadric radial basis functions. *Neural Networks*, vol. 14, pp. 185-199.

Mai-Duy, N.; Tran-Cong T. (2001) *Numerical* solution of Navier-Stokes equations using multiduadric radial basis functions. *International Journal for Numerical Methods in Fluids,* vol. 37, pp. 65-86.

Mai-Duy, N.; Tran-Cong, T. (2001): Numerical solution of Navier–Stokes equations using multiquadric radial basis function networks. *International Journal for*

Numerical Methods in Engineering in Fluids; **37**: 65–86.

Mai-Duy, N.; Mai-Cao, L.; Tran-Cong, T. (2007): Computation of transient viscous flows using indirect radial basis function networks. *CMES: Computer Modeling in Engineering and Sciences*, vol.18, pp. 59-77.

Mariani, V. C.; Alonso, E.E.M.; Peters, S. (2008): Numerical Results for a Colocated Finite-Volume Scheme on Voronoi Meshes for Navier-Stokes Equations. *CMES: Computer Modeling in Engineering and Sciences*, vol. 29, pp. 15-27.

Melenk, J. M.; Babuska, I. (1996): The partition of unity finite element method: basic theory and applications. *Computer Methods in Applied Mechanics and Engineering*, vol. 139, pp. 289–314.

Mohammadi, M. H. (2008): Stabilized Meshless Local Petrov-Galerkin (MLPG) Method for Incompressible Viscous Fluid Flows. *CMES: Computer Modeling in Engineering and Sciences*, vol.29, pp. 75-94.

Nayroles, B.; Touzot, G.; Villon, P. (1991): The diffuse approximations, *C.R. Acad. Sci. Paris Ser.* II, vol. 313, pp. 133–138.

Nayroles, B.; Touzot, G.; Villon, P. (1992): Generalizing the finite element method: diffuse approximation and diffuse elements. *Computational Mechanics,* vol. 10, pp. 307–318.

Nicolás, A.; Bermúdez, B. (2004): 2D incompressible viscous flows at moderate and high Reynolds numbers. *CMES: Computer Modeling in Engineering and Sciences*, vol. 6, pp. 441-451.

Nicolás, A.; Bermúdez, B. (2007): Viscous Incompressible Flows by the Velocity-Vorticity Navier-Stokes Equations. *CMES: Computer Modeling in Engineering and Sciences*, vol. 20, pp. 73-83.

Onate, E.; Idelsohn, S.; Zienkiewicz, O.; Taylor, R. L. (1995): A finite point method in computational mechanics application to convective transport and fluid flow. *International Journal for Numerical Methods in Engineering*, vol. 39, pp. 3839–3866.

Sanyasiraju, Y. V. S. S.; Chandhini, G. (2008): Local radial basis function based gridfree scheme for unsteady incompressible viscous flows. *Journal of Computational Physics*, vol. 227, pp. 8922–8948.

Sellountos, E. J.; Sequeira, A. (2008): An advanced meshless LBIE/RBF method for solving two-dimensional incompressible fluid flows. *Computational Mechanics*, vol. 41, pp. 617–631.

Sellountos, E. J.; Sequeira A. (2008): A Hybrid Multi-region BEM/LBEI-RBF Velocity-Vorticity Scheme for the Two-Dimensional Navier-Stokes Equations. *CMES: Computer Modeling in Engineering and Sciences*, vol. 23, pp. 127-147.

Shu, C.; Ding, H.; Yeo, K. S. (2005): Computation of Incompressible Navier-Stokes Equations by Local RBF-based Differential Quadrature Method. *CMES: Computer Modeling in Engineering and Sciences*, vol. 7, pp. 195-206.

Taylor, C.; Hood P. (1973): A numerical solution of the Navier–Stokes equations using the finite element technique. *Computers & Fluids,* vol. 1, pp. 73–100.

Weinan, E.; Liu, J. G. (1996): Vorticity boundary condition and related issues for finite difference schemes. *Journal of Computational Physics*, vol. 124, pp. 368–382.

Zhang, X.; Liu, X. H.; Song, K. Z.; Lu, M. W. (2001): Least-square collocation meshless method. *Computer Methods in Applied Mechanics and Engineering*, vol. 51, pp. 1089 –1100.

Zhu, T.; Zhang, J.; Atluri, S. N. (1998): A meshless local boundary integral equation (LBIE) method for solving nonlinear problems. *Computational Mechanics*, vol. 22, pp. 174 –186.

CMES: Computer Modeling in Engineering & Sciences

ISSN : 1526-1492 (Print); 1526-1506 (Online)

Journal website:
http://www.techscience.com/cmes/

Manuscript submission
http://submission.techscience.com

Published by
Tech Science Press
5805 State Bridge Rd, Suite G108
Duluth, GA 30097-8220, USA

Phone (+1) 678-392-3292
Fax (+1) 678-922-2259
Email: sale@techscience.com
Website: http://www.techscience.com
Subscription: http://order.techscience.com

CMES is Indexed & Abstracted in
Applied Mechanics Reviews; Cambridge Scientific Abstracts (Aerospace and High Technology; Materials Sciences & Engineering; and Computer & Information Systems Abstracts Database); CompuMath Citation Index; Current Contents: Engineering, Computing & Technology; Engineering Index (Compendex); INSPEC Databases; Mathematical Reviews; MathSci Net; Mechanics; Science Alert; Science Citation Index; Science Navigator; Zentralblatt fur Mathematik.